Progress In Electromagnetics Research M, Vol. 109, 51–61, 2022

Decoupling Control of Six-Pole Hybrid Magnetic Bearings

Gai Liu[1], Junqi Huan[1], Huangqiu Zhu[1, *], Chenyin Zhao[2], and Zhihao Ma[1]

Abstract—Six-pole hybrid magnetic bearing is a multiple input-output system with strong coupling between the degrees of freedom, a state feedback linearization dynamically decoupling the fuzzy immune PID controller for the subsystem after linear resolution coupling is proposed in this paper. Firstly, the basic theory of linear resolving coupling is expounded. Secondly, the proposed decoupling theory and control strategy are simulated in Matlab. Finally, the experimental platform is built, and the suspension experiments and coupling experiments are performed. It can be seen that the fuzzy immune PID controller has good performance, and the state feedback linearization method can realize the decoupling between the radial degrees of freedom of six-pole magnetic bearings.

1. INTRODUCTION

The friction between the rotor and stator of traditional mechanical bearing increases the energy loss, and this can be solved by magnetic bearing [1]. Traditional magnetic bearings have eight magnetic poles, and two magnetic poles are driven by one power amplifier, so magnetic bearing requires four power amplifiers [2]. A rotary shaft is supported by two radial magnetic bearings, and the rotary shaft connects with the rotor of a motor [3, 4]. Power amplifier and displacement sensors increase the cost and volume of a magnetic bearing system. Therefore, a compact and cost-effective design has long been an important issue in research and development of magnetic bearings. One approach is to use sensorless control [5–7]. Only one three-phase inverter is required for three-pole magnetic bearings in [8], which greatly reduces the cost and power consumption of a magnetic bearing system. To increase the stability of magnetic bearings, an accurate mathematical model is established in [9]. In order to perform the six-pole magnetic bearing under high speed operation, the degrees of freedom and controller must be designed for the decoupling subsystems [10].

In [11], a multivariable decoupling Fuzzy-Smith predictive control algorithm is presented, and this algorithm has a good control performance to achieve obvious decoupling between outputs and has a strong robustness. A nonlinear controller based on state feedback linearization is designed such that the nonlinear system with multivariable and strongly coupled motion is reduced to decoupled linear subsystems [12]. The decoupling control strategy based on the Internal Model Control (IMC) is proposed, and it has better decoupling and realizes dynamic decoupling control [13]. The dynamics in stator flux oriented reference frame is heavily affected by the nonlinear cross-coupling between the two axes, and a nonlinear transformation method to decouple the axes for a uniform bandwidth at all operating points is proposed to solve it [14]. The decoupled hybrid radial magnetic bearing is proposed, which can simultaneously produce radial active controllable suspension force, radial passive suspension force, and axial passive suspension force [15]. The x and y magnetic circuits of the heteropolar PM biased radial magnetic bearing are independent of each other, which decreases the magnetic field coupling of the two channels significantly [16]. A decoupling control approach based on inverse system method is

Received 24 January 2022, Accepted 15 March 2022, Scheduled 24 March 2022

* Corresponding author: Huangqiu Zhu (zhuhuangqiu@ujs.edu.cn).

[1] School of Electrical and Information Engineering Jiangsu University, Zhenjiang 212003, China. [2] State Grid Zhenjiang Electric Power Supply Company, Zhenjiang 212003, China.

developed in [17], and the inverse system compensates original system to pseudo linear system of linear transmission relationship, which can realize dynamic decoupling control among the 5 degrees of freedom of AC HMB electro-spindle.

In this paper, the state feedback linearization method is used to dynamically decouple the six-pole hybrid magnetic bearing. A fuzzy immune PID controller is designed for the linear resolving coupling subsystem, and the feasibility of the decoupling control strategy is verified by simulation and test.

2. SIX-POLE MAGNETIC BEARING STATE FEEDBACK LINEAR RESOLVING COUPLING

State feedback linearization is an important method to develop linear coupling control for nonlinear system with differential geometry. The purpose is to accurately linearize the nonlinear system and turn the system into a linear system, and linear control theory can be used to design the controller in a wide work area without losing the system accuracy and controllability. Its physical concept is clear, intuitive, and understandable. With the continuous development of digital processor technology, the designed differential geometry operation in state feedback is no longer an obstacle to its engineering applications [18].

State feedback linearization is the main part of a differential geometric control theory system. Its principle is to find a state feedback control law through the nonlinear coordinate transformation to turn the state equation of the nonlinear system into a completely controllable linear system, so that each input channel of the corresponding closed-loop system can independently control an output channel and realize the system input and output linearization. The following nonlinear systems is as follows:

$$\begin{cases} \dot{x} = f(x) + g(x)u \\ y = h(x) \end{cases} \tag{1}$$

where $x \in R^n$ is the state vector of the system; u is the input vector of the system; y is the output of the system; $f(x)$, $g(x)$, $h(x)$ is the smooth enough vector field of R^n; all the partial derivatives of $f(x)$ and $g(x)$ are defined and continuous. To linearize the input and output of the system, the output y of the system is derived.

$$\dot{y} = L_f h(x) + L_g h(x)u \tag{2}$$

where $L_f h = \frac{\partial h}{\partial x} f(x)$ and $L_g h = \frac{\partial h}{\partial x} g(x)$ are the Lie derivatives of $\mathbf{h}(\mathbf{x})$ about $\mathbf{f}(\mathbf{x})$ and $\mathbf{g}(\mathbf{x})$, respectively. To take the derivative of the system output y until at least one input component becomes explicit, the order of defining the y-derivative is its relative order. Assuming that the relative order of y is r, the formula is:

$$y^{(r)} = L_f^r h(x) + L_g^{r-1} h(x)u \tag{3}$$

The above derivative procedure is repeated for each output of the system to obtain a complete m-dimensional expression:

$$\left[y_1^{(r_1)} \dots y_m^{(r_m)} \right]^T = A(x) + E(x)[u_1 \dots u_m]^T \tag{4}$$

where

$$E(x) = \begin{bmatrix} L_{g1} L_f^{r-1} h_1(x) & \dots & L_{gm} L_f^{r-1} h_1(x) \\ \vdots & \vdots & \vdots \\ L_{g1} L_f^{r_m-1} h_m(x) & \dots & L_{gm} L_f^{r_m-1} h_m(x) \end{bmatrix} \tag{5}$$

$$A(x) = [L_f^r h_1(x) \dots L_f^{r_m} h_m(x)]^T \tag{6}$$

Among them, $E(x)$ is the decoupling matrix of the system. If $E(x)$ is a non-singular array, the following coordinate transformation can be considered:

$$u = -E^{-1}(x)A(x) + E^{-1}(x)v \tag{7}$$

In Equation (7), v is the set intermediate variable. Equation (7) is the desired state feedback control law, and the input and output map represented by Equation (4) is reduced to the integral chain form shown in the following Equation (8):

$$\left[y_1^{(r_1)} \dots y_m^{(r_m)}\right]^T = [v_1 \dots v_m]^T \tag{8}$$

The process above realizes the linear resolving coupling of the nonlinear system in Equation (1). Schematic diagram of linear resolving coupling of six-pole magnetic bearing is shown in Figure 1.

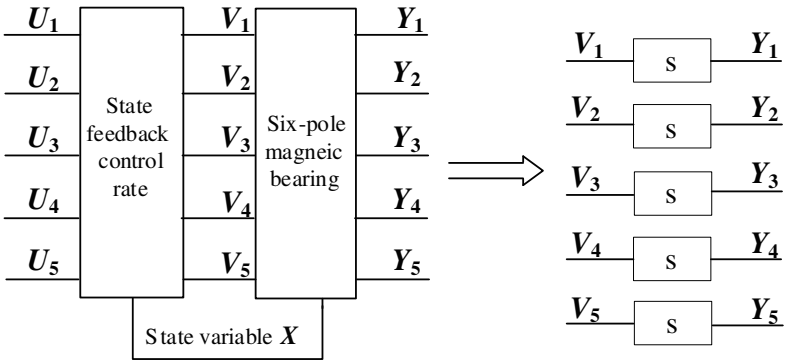

Figure 1. Schematic diagram of linear resolving coupling of six-pole magnetic bearing.

The fuzzy immune controller is designed as follows. Suppose that the number of antigens in generation k is $\varepsilon(k)$; antigen stimulation in T cells includes T_H cell and T_S cell; the output of the cells T_H is indicated by $T_H(k)$; the output of the cells T_S is indicated by $T_S(k)$; the total stimuli received by B cells can be introduced as shown in the following formula:

$$\begin{cases} S(k) = T_H(k) - T_S(k) \\ \Delta S(k) = S(k) - S(k-1) \end{cases} \tag{9}$$

where $T_H(k) = k_1\varepsilon(k)$, $T_S(k) = k_2 f[S(k), S(k)]\varepsilon(k)$, k_1 is the set stimulus factor; k_2 is the set repressor; $S(k)$ is the amount of error change for stimulated B cells. The amount of antigen $\varepsilon(k)$ is used as the deviation amount of the system $e(k)$, and the total stimulus $S(k)$ received by B cells is used as the control output of the system $u(k)$. The following feedback control law can be obtained:

$$u(k) = k_1\{1 - \eta f[u(k), \Delta u(k)]\}e(k) = K_p e(k) \tag{10}$$

where the set stimulus factor k_1 mainly controls the response speed; $\eta = k_2/k_1$ mainly determines the stability effect of the control; $f(*)$ is a selected non-linear function about $u(k)$ and $u(k)$. Since the fuzzy control can approximate any nonlinear function, this paper builds a fuzzy controller to realize the nonlinear function $f(*)$. The output $u(k)$ of the immune controller and the output rate of change $u(k)$ are used as the two inputs to the fuzzy controller, respectively, and the amount of inhibition $f(*)$ of B cells is used as the sole output of the fuzzy controller. In the fuzzy control, it is necessary to convert the exact quantitative blur to a fuzzy subset on the standard theoretic domains, so the ranges of change of the inputs $u(k)$ and $u(k)$ are defined for the fuzzy set. The fuzzy set is $\{P, N\}$; the domain range is $\{-3, 3\}$; the output $f(*)$ on the fuzzy set is as $\{P, Z, N\}$; the domain range is $\{-1, 1\}$. Block diagram of the fuzzy immune controller structure is shown in Figure 2.

The above designed fuzzy immune controller is actually a nonlinear proportional controller, which cannot effectively control the second and above systems, nor can it compensate the noise or the errors caused by external interference. The integral and differential links in the PID controller can well eliminate static difference, improve accuracy, and eliminate jitter. Therefore, this paper combines the fuzzy immune controller with the PID controller, namely the fuzzy immune PID controller.

The discrete form of the ordinary PID control algorithm can be expressed in Equation (11):

$$u_{\text{PID}}(k) = \left(k_P + \frac{k_I}{z-1} + k_D\frac{z-1}{z}\right)e(k) \tag{11}$$

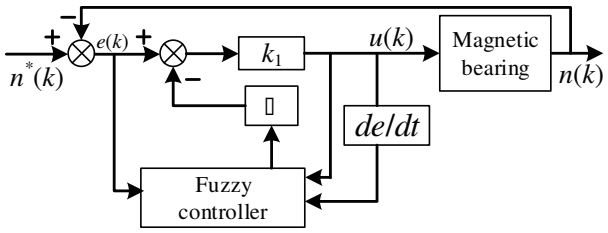

Figure 2. Block diagram of the fuzzy immune controller structure.

where k_P, k_I, and k_D are PID proportional coefficients, integral coefficient, and differential coefficient, respectively. The conventional fuzzy immune PID controller can simply connects fuzzy immune control with PID control, with the output of PID controller as the input of fuzzy immune controller, combined with Eqs. (10) and (11) can launch the output of fuzzy immune PID controller as:

$$\begin{aligned} U(k) &= k_1\{1-\eta f[u(k)\Delta u(k)]\}\cdot u_{\mathrm{PID}}(k) \\ &= \left(K_P + \frac{K_I}{z-1} + K_D\frac{z-1}{z}\right)e(k) \end{aligned} \tag{12}$$

where K_P, K_I, K_D are

$$\begin{cases} K_P = k_P k_1\{1-\eta f[u(k),\Delta u(k)]\} \\ K_I = k_I k_1\{1-\eta f[u(k),\Delta u(k)]\} \\ K_D = k_D k_1\{1-\eta f[u(k),\Delta u(k)]\} \end{cases} \tag{13}$$

As can be seen from Equation (13), when the three coefficients of the PID K_P, K_I, K_D are fixed cases, the change of K_P, K_I, K_D will only simultaneously enlarge or shrink the same proportion simultaneously, but each change of K_P, K_I, K_D has a different effect on the performance of the system. It can be seen that the fuzzy immune control is connected with the ordinary PID control, and the parameters that meet the control performance are difficult to adjust quickly. The precise adjustment is bound to affect the control effect of the system. In view of this problem, this paper uses the fuzzy adaptive PID in series with the fuzzy immune controller, which can solve the problem of K_P, K_I, and K_D in adjustment, so as to realize the controller parameter accuracy, automatic tuning, improve the control quality, and improve the system performance. The frame diagram of the improved fuzzy immune PID controller structure is shown in Figure 3.

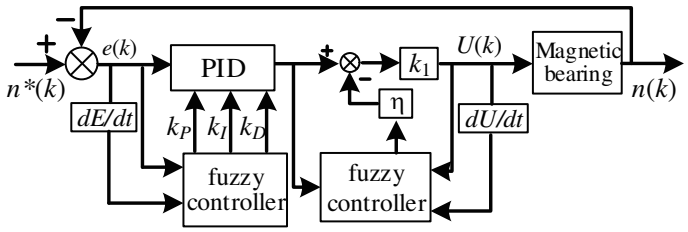

Figure 3. The frame diagram of the improved fuzzy immune PID controller structure.

The fuzzy PID uses a Mamdani-type 2-D fuzzy controller, taking the error $e(k)$ as well as the rate of change of the error $\Delta e(k)$ as the input of the fuzzy controller. The outputs k_P, k_I, and k_D are respectively used as the three coefficients of PID.

The variation ranges of $e(k)$, $\Delta e(k)$, k_P, k_I, k_D changes are defined for the fuzzy set of standard theory domains separately by quantifying the factors. The domain range is $\{-3,-2,-1,0,1,2,3\}$, and the fuzzy set is $\{\mathrm{NB},\mathrm{NM},\mathrm{NS},\mathrm{ZO},\mathrm{PS},\mathrm{PM},\mathrm{PB}\}$. To ensure the accuracy and flexibility of the control, all the fuzzy language variables use the more sensitive and relatively simple triangle membership functions. The inference rules of the input fuzzy value to the input fuzzy value are established based on the

Table 1. Fuzzy rules table of the k_P.

$E(k)$ \ $\Delta E(k)$ (k_I)	NB	NM	NS	ZO	PS	PM	PB
NB	NB	NB	NM	NM	NS	ZO	ZO
NM	NB	NB	NM	NS	NS	ZO	ZO
NS	NB	NM	NS	NS	ZO	PS	PS
ZO	NM	NM	NS	ZO	PS	PM	PM
PS	NM	NS	ZO	PS	PS	NM	PB
PM	ZO	ZO	PS	PS	PM	PB	PB
PB	ZO	ZO	PS	PM	PM	PB	PB

Table 2. Fuzzy rules table of the k_I.

$e(k)$ \ $\Delta e(k)$ (k_P)	NB	NM	NS	ZO	PS	PM	PB
NB	PB	PB	PM	PM	PS	ZO	ZO
NM	PB	PB	PM	PS	PS	ZO	NS
NS	PM	PM	PM	PS	ZO	NS	NS
ZO	PM	PM	NB	ZO	NS	NM	NM
PS	PS	NB	ZO	NS	NS	NM	NM
PM	PS	ZO	NS	NM	NM	NM	NB
PB	ZO	ZO	NM	NM	NM	NB	NB

Table 3. Fuzzy rules table of the k_D.

$E(k)$ \ $\Delta E(k)$ (k_D)	NB	NM	NS	ZO	PS	PM	PB
NB	PS	NS	NB	NB	NB	NM	PS
NM	PS	NS	NB	NM	NM	NS	ZO
NS	ZO	NS	NM	NM	NS	NS	ZO
ZO	ZO	NS	NS	NS	NS	NS	ZO
PS	ZO	ZO	ZO	ZO	ZO	ZO	ZO
PM	PB	NS	PS	PS	PS	PS	PB
PB	PB	PM	PM	PM	PS	PS	PB

experimental experience, and the fuzzy control rule tables of k_P, k_I and k_D are shown in Table 1, Table 2, and Table 3, respectively.

3. SIMULATION TEST AND PERFORMANCE ANALYSIS

To verify the decoupling strategy and control method, the object of the six-pole magnetic bearing test prototype is conducted by Matlab/Simulink. The parameters of six-pole hybrid magnetic bearings are designed and listed in Table 4.

The axial single DOF magnetic bearings is used to verify the performance of the fuzzy immune PID controller. Figure 4 is a simulation block diagram of a single degree of freedom magnetic bearing using a fuzzy immune PID controller. Figure 5 is a simulation block diagram of fuzzy PID and its submodules in Figure 4. Figure 6 is a block diagram of fuzzy immune units and its sub-module simulation block diagram in Figure 4.

Figure 7 is a floating diagram of an axial single-degree of freedom magnetic bearing under different controllers, from an initial position of 0 mm and suspended to an equilibrium position of 0.15 mm. It can be seen that the controller adopted in this paper has no overshoot, no static difference, and the adjustment speed is fast.

Simulation test is conducted with the radial two-degrees of freedom hybrid magnetic bearing as the object. The balance position of the rotor is 0 mm. An external disturbance force lasting 0.1 s is suddenly added when the rotor is stably suspended. Figures 8 and 9 are the axial movement trajectory of the radial two-degrees of freedom hybrid magnetic bearing under different controllers, respectively. It can be seen that the traditional PID control is relatively large, while the axial trajectory arc is significantly reduced, and the motion range is reduced under the improved fuzzy immune PID control.

Table 4. Parameters of six-pole hybrid magnetic bearings.

Parameters	Six-pole hybrid magnetic bearings
The position stiffness N/mm	240.8
The current stiffness N/A	227.3
The mass of the rotor m/kg	5
Radial air gap length l/mm	0.5
Saturation induction density B_S/T	0.8
The area of radial magnetic pole S/mm^2	320
The max ampere-turns of radial coils/At	140
Magnetomotive force of PM F_m/At	280
Outer diameter of stator yoke d_1/mm	82
Inter diameter of stator yoke d_2/mm	58
Thickness of stator l_1/mm	10
Outer diameter of rotor d_3/mm	144
Inter diameter of rotor d_4/mm	118
Thickness of rotor l_2/mm	23
Outer diameter of PM d_5/mm	72
Inter diameter of PM d_6/mm	58
Axial length of PM l_3/mm	3

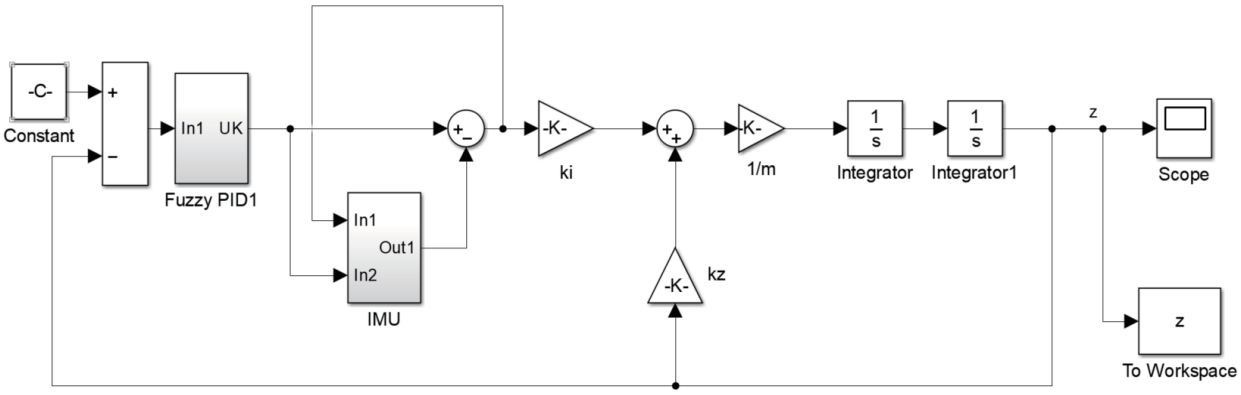

Figure 4. Simulation block diagram of a single degree of freedom magnetic bearing using a fuzzy immune PID controller.

4. PROTOTYPE AND EXPERIMENT

In order to verify the accuracy of the above analysis results and further analyze the performance of the six-pole magnetic bearing, an experimental platform is designed and manufactured as shown in Figure 10. The experimental platform is mainly composed of eddy current displacement sensor, displacement signal interface circuit, DSP controller minimum system, DC power supply, radial power drive board, axial power drive board, AC power supply, PC machine, and DSP controller.

The six pole magnetic bearing state feedback linear resolved coupling control block diagram is shown in Figure 11. The six pole magnetic bearing system is decoupled by the state feedback linearization, and the fuzzy immune PID controller is coupled in the control loop of each decoupling subsystem to achieve high performance control of the six pole magnetic bearings. In the state feedback linearly decoupling,

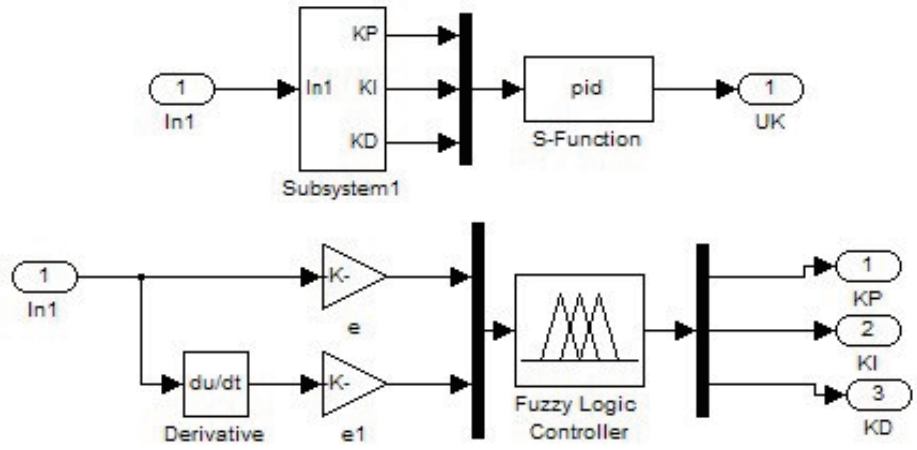

Figure 5. Simulation block diagram of the fuzzy PID and its submodules.

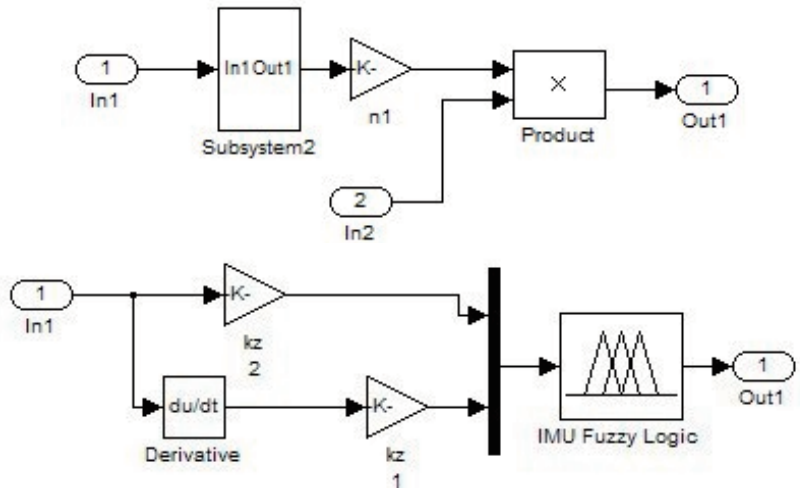

Figure 6. Simulation block diagram of the fuzzy immune unit and its submodules.

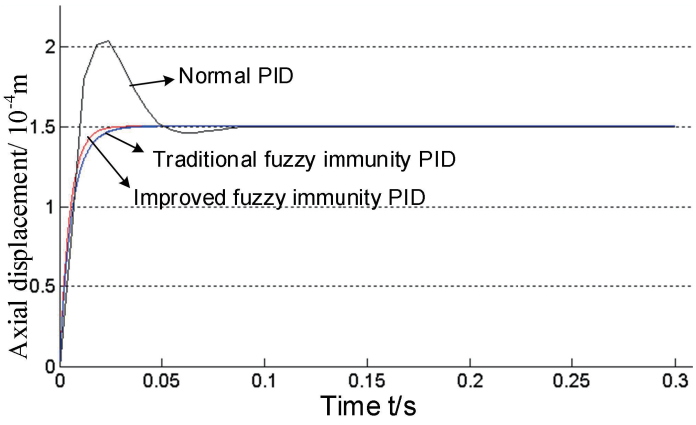

Figure 7. Floating of axial single DOF magnetic bearing under different controllers.

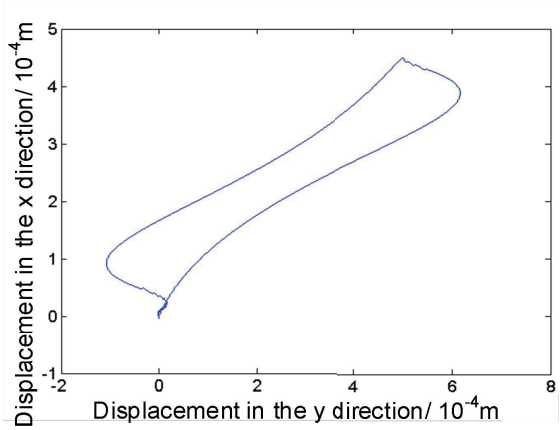

Figure 8. Axis trajectories under the conventional PID.

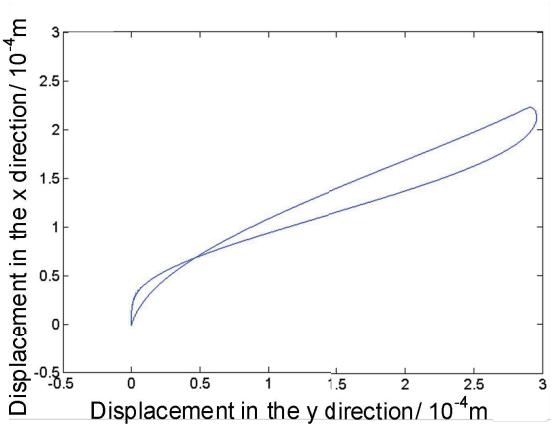

Figure 9. Improved axial trajectories under fuzzy immune PID.

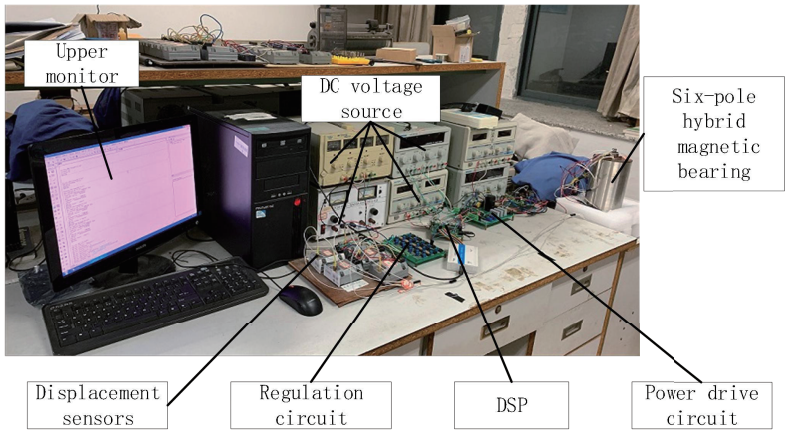

Figure 10. Experimental platform.

the differential equations of the control system are listed, and the eigenvalue and eigenvectors of the coefficient matrix are obtained. The matrix is changed to the diagonal matrix, and the transformation is replaced back to the original system for decoupling. Simulation tests were performed in Matlab to validate the decoupling control strategy described above.

4.1. Rotor Lifting Test

The comparison of the centroid trajectories at the rotor of six-pole magnetic bearing is shown in Figure 12. The x coordinate is x direction displacement; y coordinate is time; and z coordinate is y direction displacement. Figure 12(a) is centroid trajectories at the three-degrees of freedom magnetic bearing; the rotor centroid is in a static state at the initial moment; and the displacement in x and y direction is set to 0 mm. After 0.1 s, the displacements of rotor centroid in x and y direction are 1.5 mm and 1.5 mm, and the rotor realizes stable suspension. By comparing the centroid trajectories of the rotor before and after decoupling, the rotor reaches a stable suspension state, and the vibration is small after decoupling. Figure 12(b) shows centroid trajectories at the two-degrees of freedom magnetic bearing, and the shaking of the rotor before decoupling is large when it is reaching the steady state, but the centroid trajectory of the rotor after decoupling is smooth. Figure 12 shows that the decoupled rotor centroid floating trajectory is smoother with less vibration and better dynamic and static performance than that before uncoupling.

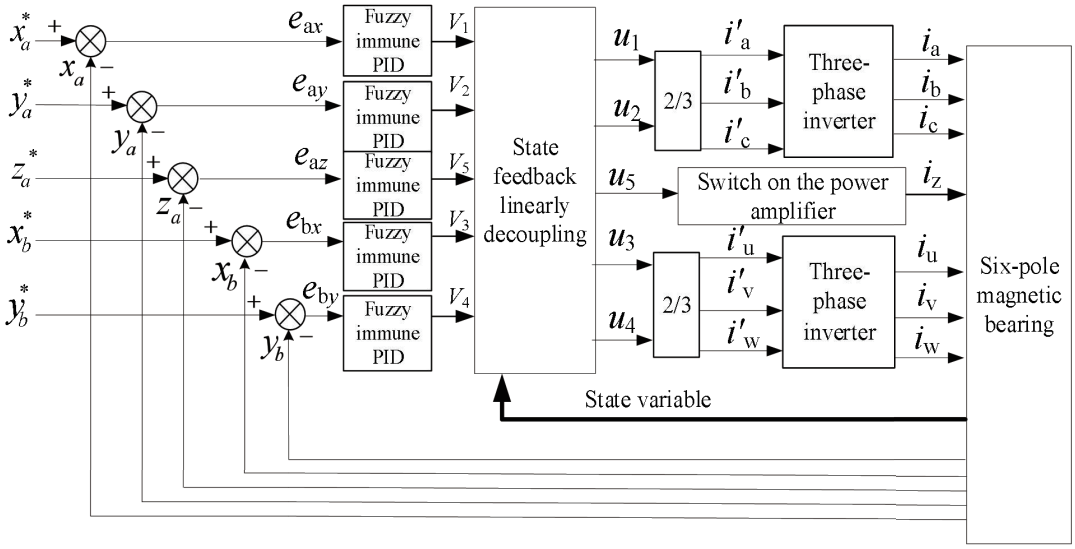

Figure 11. The six pole magnetic bearing state feedback linear resolved coupling control block diagram.

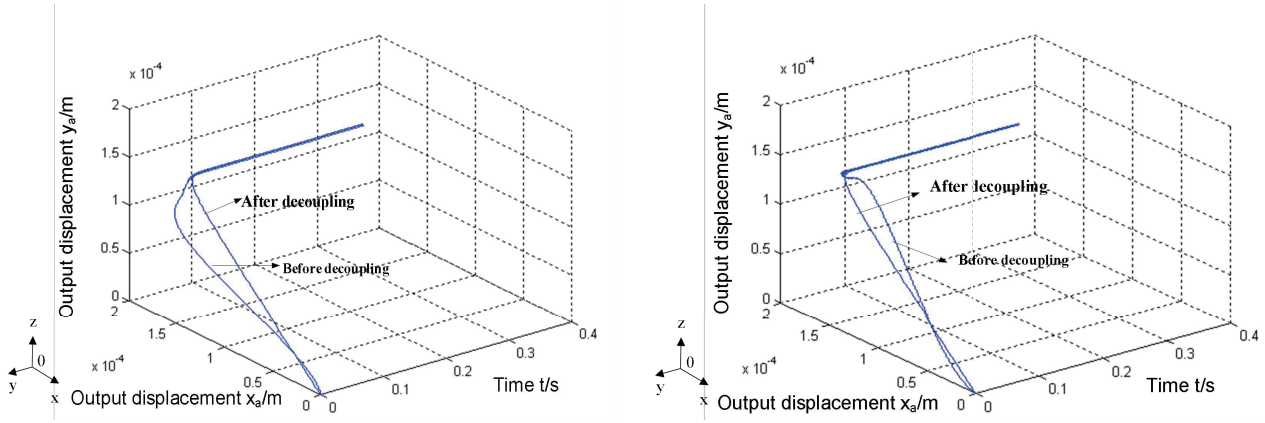

Figure 12. Comparison of rotor centroid float trajectories before and after decoupling. (a) The centroid trajectories of the three-degrees of freedom. (b) The centroid trajectories of the two-degrees of freedom.

4.2. Analysis of Decoupling Effect

There is no electrical coupling between the axial and other four radial degrees of freedom in the control system, so the decoupling effect between the radial four degrees of freedom is analyzed. The desired rotational speed of the rotor is $n = 10,000\,\mathrm{r/min}$, with a 100 N interference force for 0.02 s to the displacement curve and the two degrees of freedom magnetic bearing in x_a, y_a, x_b and y_b as shown in Figures 13(a), 13(b), 13(c), 13(d). As can be seen in Figure 13(a), the rotor is in the equilibrium position, and external interference is added at the time of 0.15 s. The displacement of the rotor in the x_a direction suddenly becomes larger. The external interference duration withdraws after 0.02 s, and at this time, the rotor is near its original position and returns to the equilibrium position in a very short time. The time of the rotor under the external interference while it returns to the equilibrium position in the x_a direction is 0.02 s in Figure 13(a). The time of the rotor under the external interference while it returns to the equilibrium position in the y_a direction is 0.04 s in Figure 13(b). The time of the rotor under the external interference while it returns to the equilibrium position in the x_b direction is 0.005 s

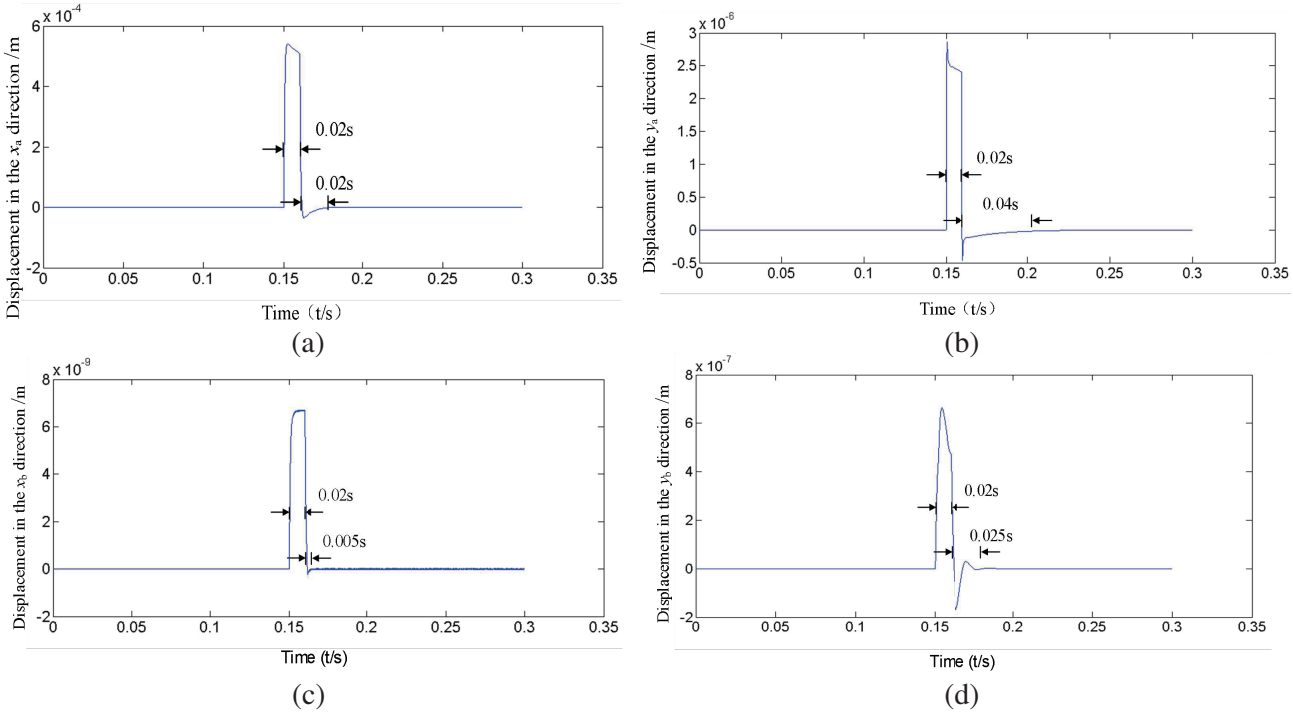

Figure 13. Displacement curves of the x_a, y_a, x_b, y_b direction with interference forces in the x_a direction.

in Figure 13(c). The time of the rotor under the external interference while it returns to the equilibrium position in the y_b direction is 0.025 s in Figure 13(d). It can be seen from Figure 13 that the coupling between radial degrees of freedom is small, and the dynamic uncoupling is well realized.

5. CONCLUSION

This paper expounds the basic theory of linear resolving coupling. The theory is used to realize the decoupling of the five degrees of freedom of the six-pole hybrid magnetic bearing, according to the problem of difficult parameters of traditional fuzzy immune PID controller. A control algorithm combining fuzzy immune control with fuzzy adaptive PID control was used and strung in the control loop of each post-decoupled subsystem. The decoupling theory and the control strategy proposed in Matlab/Simulink show that the fuzzy immune PID controller has good performance, and the state feedback linearization method can realize the decoupling between the radial degrees of freedom of six-pole magnetic bearings.

REFERENCES

1. Gu, H., H.-Q. Zhu, and Y.-Z. Hua, "Soft sensing modeling of magnetic suspension rotor displacements based on continuous hidden markov model," *IEEE Transactions on Applied Superconductivity*, Vol. 28, No. 3, 1–5, 2018.
2. Wu, C. and H.-K. Zhang, "Finite element analysis of eight-pole homopolar hybrid magnetic bearing," *2021 IEEE International Conference on Electrical Engineering and Mechatronics Technology (ICEEMT)*, 156–160, 2021.
3. Usman, I., M. Paone, K. Smeds, et al., "Radially biased axial magnetic bearings/motors for precision rotary-axial spindles," *IEEE/ASME Transactions on Mechatronics*, Vol. 16, No. 3, 411–420, 2011.

4. Abooee, A. and M. Arefi, "Robust finite-time stabilizers for five-degree-of-freedom active magnetic bearing system," *Journal of the Franklin Institute-Engineering and Applied Mathematics*, Vol. 356, 80–102, 2019.
5. Peng, C., J. Sun, X. Song, and J. Fang, "Frequency-varying current harmonics for active magnetic bearing via multiple resonant controllers," *IEEE Transactions on Industrial Electronics*, Vol. 64, No. 1, 517–526, 2017.
6. Liu, G. and H.-Q. Zhu, "Displacement estimation of six-pole hybrid magnetic bearing using modified particle swarm optimization support vector machine," *Energies*, Vol. 15, No. 5, 2022.
7. Yu, J. and C. Zhu, "A multifrequency disturbances identification and suppression method for the self-sensing AMB rotor system," *IEEE Transactions on Industrial Electronics*, Vol. 65, No. 8, 6382–6392, 2018.
8. Zhang, W.-Y., H.-Q. Zhu, Z.-B. Yang, et al., "Nonlinear model analysis and 'switching model' of AC-DC three degree of freedom hybrid magnetic bearing," *IEEE/ASME Transactions on Mechatronics*, Vol. 21, No. 2, 1102–1115, 2016.
9. Zhang, W.-Y., H.-K. Yang, L. Cheng, et al., "Modeling based on exact segmentation of magnetic field for a centripetal force type-magnetic bearing," *IEEE Transactions on Industrial Electronics*, Vol. 67, No. 9, 7691–7701, 2020.
10. Ren, L.-M. and K.-K. Wang, "A moment and axial force sensor using a self-decoupled, passive and wireless method," *IEEE Sensors Journal*, Vol. 21, No. 19, 21432–21440, 2021.
11. Zhao, J.-H. and F. Han, "Decoupling control of multi-DOF supporting system of MLDSB," *Applied Sciences-Basel*, Vol. 11, No. 16, 2021.
12. Sun, X., H. Zhu, and L. Dang, "Linearization decoupling control of bearingless induction motor based on rotor field oriented control," *2019 IEEE 3rd Information Technology, Networking, Electronic and Automation Control Conference (ITNEC)*, 11–15, 2019.
13. Zhang, T. and J. Zhen, "Suspension performance analysis on the novel hybrid stator type bearingless switched reluctance motor," *IEEE Transactions on magnetics*, Vol. 57, No. 6, 2021.
14. Varatharajan, A., G. Pellegrino, and E. Armando, "Direct flux vector control of synchronous motor drives: Accurate decoupled control with online adaptive maximum torque per ampere and maximum torque per volts evaluation," *IEEE Transactions on Industrial Electronics*, Vol. 69, No. 2, 1235–1243, 2022.
15. Li, S.-P., L.-W. Song, J.-Y. Wang, S.-Z. Li, and X.-F. Lei, "Decoupling active and passive hybrid radial magnetic bearing," *2015 International Conference on Control, Automation and Information Sciences (ICCAIS)*, 1–6, 2015.
16. Xu, S.-L. and J.-J. Sun, "Decoupling structure for heteropolar permanent magnet biased radial magnetic bearing with subsidiary air-gap," *IEEE Transactions on Magnetics*, Vol. 50, No. 8, 1–8, 2014.
17. Yang, Y.-F, Y. Ruan, W. Zhang, Q. Wang, Z.-B. Yang, and H.-Q. Zhu, "Decoupling control of 5 degrees of freedom AC hybrid magnetic bearings based on inverse system method," *Proceedings of the 30th Chinese Control Conference*, 278–282, 2011.
18. Kandil, A. and Y.-S. Hamed, "Tuned positive position feedback control of an active magnetic bearings system with 16-poles and constant stiffness," *IEEE ACCESS*, Vol. 9, 73857–73872, 2021.